Journal of The Electrochemical Society





# Surface Alloying During Pb Underpotential Deposition on Au(111)

*Journal of The Electrochemical Society*, 2022 **169** 112509

# Surface Alloying During Pb Underpotential Deposition on Au(111)

**Alicja Szczepanska**[1,2] and **Natasa Vasiljevic**[1,2,*,z]

[1]*School of Physics, H.H. Wills Physics Laboratory, University of Bristol, Bristol, BS8 1TL, United Kingdom*
[2]*Bristol Centre for Functional Nanomaterials, University of Bristol, Bristol, BS8 1TL, United Kingdom*

The surface alloying during Pb underpotential deposition (UPD) on Au(111) films was studied using electrochemical techniques. This UPD system has been known for its unusual stress behavior associated with surface alloying during epitaxial monolayer (ML) formation. The characteristic cyclic voltammetry of Pb UPD on Au(111) exhibits an anodic peak at the most positive potentials that does not have a symmetric cathodic counterpart. The peak can be associated with the surface structural changes due to the Pb dealloying from the top substrate layer. Two electrochemical approaches were used to study the surface transformations: i) extended polarization (up to 60 min) at high Pb coverage of 0.85 ML, and ii) repeated cycling 1150 times between the potentials corresponding to 0.25 ML and 1 ML Pb coverages. In both approaches, it was observed that with the increased time of polarization or number of potential cycles, the prominent UPD peaks gradually reduced in magnitude, became broader and lost their original double-peaks structure. At the same time, the dealloying (the most anodic) peak shifted positive about 0.1 V and increased in magnitude. Quantitative analysis of the changes estimated the coverage of Pb alloying with a surface of 0.28–0.30 ML.
 [DOI: 10.1149/1945-7111/aca0c3]

Manuscript submitted September 8, 2022; revised manuscript received October 30, 2022. Published November 16, 2022. *This paper is part of the JES Focus Issue on Nucleation and Growth: Measurements, Processes, and Materials.*

Supplementary material for this article is available online

Alloying between two metal components is driven by the negative enthalpy of mixing and lowering of the surface free energy. However, when confined to a few top surface layers, this process can be observed even in systems that do not form bulk alloys (so-called immiscible systems).[1,2] Ultra high vacuum (UHV) studies at elevated temperatures have found that the formation of surface alloys is a common phenomenon in immiscible systems with a large lattice mismatch driven by a surface stress relaxation and an elastic energy minimization.[2]

The Pb/Au system is immiscible and has a very large atomic mismatch of 21%. In the UHV environment, early surface science studies (in the 1970s) showed spontaneous surface alloying between Pb and Au for (100), (110) and (111) Au planes.[3–6] The Pb deposition on Au(111) in UHV has been studied with Low-Energy Electron Diffraction (LEED),[5–7] Auger Electron Spectroscopy (AES),[5,6] Scanning Tunnelling Microscopy (STM),[7] Angle-Resolved Photoemission Spectroscopy (ARPES),[7] Transmission Electron Microscopy (TEM) and electron diffraction.[4,8] Early studies have shown that deposition of Pb on reconstructed Au(111) lifted the reconstruction,[5,6] and started by forming an ordered structure at sub-monolayer coverages. This structure was initially interpreted as $p(\sqrt{3} \times \sqrt{3})R30°$,[5] and in later studies, it was observed on densely packed islands,[9] followed by $p(2 \times 2)$ structure formation.[6] A complete epitaxial Pb ML was found to be compressed by 0.5% with respect to bulk Pb and consisted of two equivalent domains rotated ±5° with respect to the Au substrate.[6,7] The structure was in agreement with later observations of the Moiré unit cell $(5.77 \times 5.77)R21.5°$ with respect to the Au(111) substrate.[7] AES and electron diffraction studies showed that depending on the thickness and the temperature, the ML of Pb is followed by intermetallic compounds formation such $AuPb_2$ or $Au_2Pb$.[4–6,8]

In contrast to the UHV studies, surface alloying in the electrochemical environment has been reported only for Pb underpotential deposition (UPD) on Au(111) single crystal face.[10,11] The Pb UPD on Au(111) is one of the most extensively studied UPD systems.[10–32] It has been considered a model system often used to evaluate the crystal structure and surface area of Au substrates (flat and porous electrodes)[33] and employed in the calibration of many electrochemical techniques. Even though many early reports studied the irreversibility of this UPD process,[15,19,20,26,27] the possible surface alloying between Pb and Au has not been considered. The most positive anodic peak in cyclic voltammetry is an unusual irreversible feature of this system interpreted by various processes, such as (i) surface reconstruction leading to more stable adsorbate states;[15] (ii) the removal of Pb atoms from Au(111) terraces;[19] (iii) stripping of the irreversibly deposited Pb from the Au inter-crystalline boundary sites;[17] or (iv) a change in the Au *d*-band structure due to adsorption.[34]

The in situ surface X-ray Scattering (SXS) studies of a complete Pb ML on Au(111) at an underpotential of 0.07 V reported an incommensurate, hexagonal monolayer compressed by 0.7% with respect to bulk Pb.[35] This agreed with the change in Pb-Au distance over the same potential region observed with the surface X-ray differential diffraction technique.[36] The rotation angle between Pb-UPD adlayer and Au substrate was measured to be 2.5° at underpotentials lower than 0.13 V and no rotation was observed at underpotentials higher than 0.16 V.[27] These results are in agreement with the presence of the Moiré pattern observed by the in situ STM[24,25,37] and in situ Atomic Force Microscopy (AFM).[26]

The structure of a partial Pb monolayer during UPD on Au(111) has been proposed to be $(\sqrt{3} \times \sqrt{3})R30°$.[13] However, in situ STM studies by Green et al.[24,25] showed that this structure did not form during potential sweep experiments. Moreover, they observed roughening of the Au substrate following anodic dissolution (removal) of the Pb UPD monolayer illustrated by the formation of monolayer high islands and pits. Such morphological changes have been considered an indirect confirmation of surface alloying and have been observed in other UPD systems.[38–47] Similar findings were reported in later studies[23–25] and in situ STM studies in our group.[11]

The early in situ stress measurements during Pb UPD on Au(111) reported an unusual transition of the stress change, which attracted a lot of interest.[10,11,28,29,31,48,49] One of the earliest interpretations of the observed tensile-compressive transition ("hump") in the region of the main UPD peak was attributed to the strain accommodation of the incommensurate *hcp* Pb adlayer by 2.5° rotation.[28,48,49] However, a discrepancy of about 0.07 V between the adlayer rotation and stress relaxation potentials indicated no direct relationship between them. Another explanation of the tensile rise ("hump") was the growth of the islands on terraces up to the point of their coalescence.[29] This conclusion was based on the agreement between the stress relaxation magnitude and the value calculated by a simple elastic model developed for three-dimensional island coalescence.

*Electrochemical Society Member.
[z]E-mail: n.vasiljevic@bristol.ac.uk

More recent studies implied that the stress relaxation hump at the transition between sub-monolayer to monolayer resulted from kinetically controlled surface alloying and dealloying processes.[10,11]

Surface alloying during the UPD has been reported in many other systems, such as Pb/Ag(111),[50–57] Pb/Cu(100),[42,43,58] Ag/Au(111),[59,60] Cd/Au,[44,45,61–64] Cd/Ag,[46,47,64,65] Tl/Au,[39,66] Tl/Ag(111),[38] Sn/Au(100),[40] Sn/Cu(111)[41] and Pd/Au.[67,68] Surface alloying in these systems has been observed by in situ STM[38–47] and in situ AFM[61–63,69] through the roughening or reconstruction of the substrates; or electrochemically by observing changes in shape, charge, and position of the UPD peaks. In the latter case, the changes were examined by applying a constant polarization potential for an extended time, followed by a potential sweep in the anodic or cathodic direction. Comparison of the UPD peaks obtained by such linear sweeps with those obtained on the initial surface before the polarization can indicate surface structural and compositional changes associated with surface alloying. This method has been used in the studies of surface alloying in many systems, such as Pb/Ag,[50–52,54–57] Cd/Au(100),[62,63] Cd/Ag,[46,47,64,65] Tl/Au,[66] Tl/Ag(111),[38] Pd/Au,[67,68] Pb/Cu(111),[70] also including the early studies in Pb/Au(111) system of our interest.[15] Another technique is multiple potential cycling in the limited potential region, such as the one performed on the Ag/Au (111) system.[59,60]

In this paper, we revisited Pb UPD on Au(111) system to examine the surface alloying and to demonstrate that the most positive anodic peak can be associated with the surface structural changes due to the Pb dealloying from the top substrate layer. We conducted the first in-depth electrochemical studies using two methods: 1) potential polarization at the constant underpotential of 0.2 V corresponding to 0.85 ML Pb coverage and 2) repeated cycling between the underpotentials of 0.0 V and 0.5 V corresponding to 1 ML and 0.25 ML Pb coverages respectively. The changes of UPD voltammetric peaks (shape, position, and charges) in both methods were consistent with the surface structural transformations due to the surface alloying. Following peaks evolution with time or the number of CV cycles, we examined and quantified the extent of surface changes.

## Experimental

***Material and methods.***—Electrochemical experiments were done in a standard three-electrode cell using a BioLogic VSP potentiostat (Bio-Logic Science Instruments SAS) with built-in EC-Lab software or CompactStat.h potentiostat (Ivium Technologies) with built-in IviumSoft software.

A solution of 1 mM $Pb(ClO_4)_2$ and 0.1 M $HClO_4$ was prepared using high-purity chemicals ($PbCO_3$, 99.999%, Alfa Aesar and 70% $HClO_4$, 99.9985%, Alfa Aesar). Before measurements, the solution was deaerated with the oxygen-free nitrogen gas (Oxygen Free Nitrogen, BOC) for at least 30 min. The oxygen-free environment was preserved during experiments with nitrogen flow above the solution.

A counter electrode (CE) and a pseudo-reference electrode (RE) were made of Pt (Pt80/Ir20, Advent Research Materials) and Pb (99.9%, Advent Research Materials) wires, respectively. The electrodes were sealed in glass rods for easy mounting into the electrochemical cell using glass stoppers with screw caps. Before each experiment, the electrodes were cleaned with $HNO_3$ (≥65%, Sigma Aldrich) for 10 s, rinsed with Milli-Q water (Millipore/Merck) and dried with nitrogen. The Pt wire was additionally flame annealed with a butane torch. All the potentials reported in this paper are presented with respect to the Pb pseudo-RE (Pb/$10^{-3}$M $Pb^{2+}$), with the potential being equal to −0.215 V vs Standard Hydrogen Electrode (SHE).

***Au(111) substrate surface.***—Working electrodes (WE) were ultra-high vacuum evaporated 250 nm thin films of Au with a 4 nm Ti adhesion layer on a Schott, Nexterion® Glass B (BOROFLOAT® 33) slides. The Au films/glass slides were diamond-cut rectangles of dimensions (10 mm × 25 mm). The Au substrates were prepared first by cleaning in conc. $H_2SO_4$ (95.0%–97.0%, Sigma-Aldrich) for 10 min, rinsed with Milli-Q water and dried with nitrogen. A surface with dominant (111) orientation was obtained by flame annealing for 2 min using a butane torch, then cooling in air and rinsing with Milli-Q water. The high quality of annealed Au(111) film surfaces was confirmed by X-ray diffraction (XRD) and AFM images, as shown in Figs. S1 and S2.

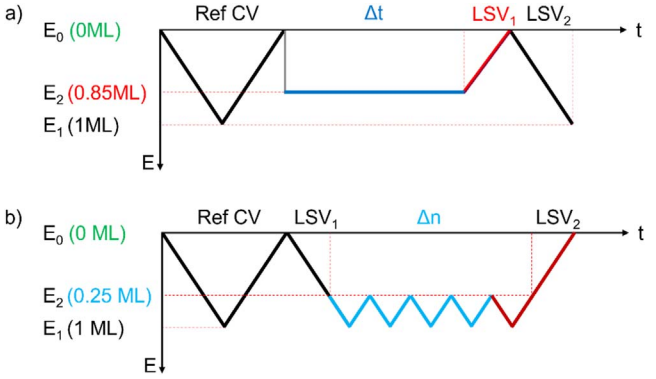


**Figure 1.** Schematic diagrams of the experimental protocols followed during (a) polarization experiments and (b) dynamic alloying (repeated cycling).

The Au sample was then mounted on the sample holder (a metal rod with an alligator clip at the end) and immediately lowered into the solution. The sample holder was mounted through the Teflon 24/40 Joint adapter, secured with an O-ring and compression cap sealing off the electrochemical cell from the environment. The first step of all electrochemical experiments was to confirm the Au substrate quality via surface oxidation/reduction, which was also used to measure the electrochemical active surface area (ECASA).[71] The Au surface was examined by cyclic voltammetry in the solution of 1 mM $Pb(ClO_4)_2$ + 0.1 M $HClO_4$ in the potential range from 0.9 V to 1.85 V, as shown in Fig. S3. Starting from the open-circuit potentials of bare Au surface toward more positive potentials, the process of electrochemical Au surface oxidation and reduction is illustrated together with the effect of flame annealing on the dominant (111) crystal structure. Before flame annealing (blue curve, Fig. S3a), Au oxidation sharp positive peak can be seen at 1.5 V with a shoulder at higher potentials, characteristic of a polycrystalline Au substrate. After the flame annealing (red curve, Fig. S3a), the peak at 1.7 V indicates the surface dominant Au(111) orientation. The cathodic peak at 1.3 V is the Au oxide reduction peak. Using a charge of 444 $\mu$C $cm^{-2}$ for an ideal Au(111),[71–73] an integrated charge under the reduction peak was normalized to calculate the sample's surface area.

***Pb UPD on Au(111).***—Figure S3b illustrates differences of Pb UPD on Au film before flame annealing (blue curve), with peaks characteristic of a polycrystalline Au substrate,[15] and after the flame annealing (red curve) exhibiting features characteristic for Au(111) surface.[14,19,20] The Pb coverage was measured by integrating the deposition and dissolution currents normalized by a charge of 302 $\mu$C $cm^{-2}$ corresponding to 1 ML of the perfect (111) surface. The charge of 1 ML of Pb UPD was also measured by chronoamperometry (CA). The integration of the first 0.6 s of the current-time transients was done for each potential step from 0.9 V (no deposition, 0 ML) to 0.0 V (full Pb coverage of 1 ML) and then from 0.0 V to 0.9 V. These charges/coverages were presented as the adsorption and desorption isotherms, respectively.

*Extended polarization experiments* were done at the potential of 0.2 V (corresponding to 0.85 ML) for 15 min and 60 min The potential was then swept in the anodic direction, followed by a cathodic sweep with scan rates of 10 mV $s^{-1}$. The schematic diagram of the experimental procedure of polarization is shown in Fig. 1a.

*The potential cycling experiments* were performed between 0.5 V and 0.0 V, corresponding to 0.25 ML and 1.00 ML Pb coverages. The potential was cycled up to 1150 times with a scan rate of 10 mV $s^{-1}$. After every few hundred cycles, the potential was swept from 0.0 V to 0.9 V, and the linear sweep was recorded for comparison with the initial CV scan. The schematic diagram of the experimental procedure for the dynamic alloying is shown in Fig. 1b.

## Results and Discussion

***Pb UPD on Au.***—Figure 2 shows the CVs of Pb UPD on Au (111). The unusual nature of this UPD system is illustrated on a set of scans with different potential limits. Figure 2a shows CVs with varied negative potential limits, and Fig. 2b with varied positive potential limits.

The gradual increase of the potential range in Fig. 2a allows us to observe the potentials at which peaks appear (at different stages of layer formation) and their associated anodic counterparts. The peaks in Fig. 2a are labelled accordingly in the order of their appearance, starting from the bare Au surface at the potential of 0.9 V. The first stage of UPD is the formation of peak C1 with its counterpart A1 (green line in Fig. 2a), which according to the previous studies, presents the random deposition at the step edges.[19] The second peak labelled C2 and its counterpart A2 are unusual. As shown in Fig. 2a, peak A2 appears as a counterpart after the potential scan below 0.4 V. The peak C2 is not a clearly defined peak but a potential plateau in the region between 0.22 V and 0.35 V with a small peak at the foot of a sharp prominent peak. The peak A2 at a potential of 0.65 V is characteristic of Pb dissolution from Au(111) and is not observed for other main Au(*hkl*) orientations.[15,20] Our observations agree with the previous studies reported for Pb UPD on Au(111).[14,15,19,20] Most UPD systems have reversible dynamics, where the deposition peaks have their dissolution counterparts in nearly the same potential range. An unusually large potential difference between C2 and A2 peaks of 0.35 V and the order of appearance are strong indications of surface dealloying and we will refer to A2 as "dealloying peak." Extending the potential limits more negatively beyond 0.22 V a dominant (sharp) peak C3 can be observed, attributed to the Pb deposition on the Au(111) terraces.[24] The corresponding dissolution peak A3 in the anodic scan has a distinctive double-peak (split peak) structure. The double-peak structure of A3 evolves and becomes more defined as the Pb coverage increases. A complete ML of Pb is present on the surface after the C3 is fully formed (between 0.15 V and 0 V). The double-peak structure, such as A3, is often interpreted as the dissolution from two energetically different sites/types of regions on the surface, e.g. terraces and steps. Also, the structure of A3 does not fully "match" the structure of the C3 peak. Further insight is obtained by CVs shown in Figs. 2b and 3.

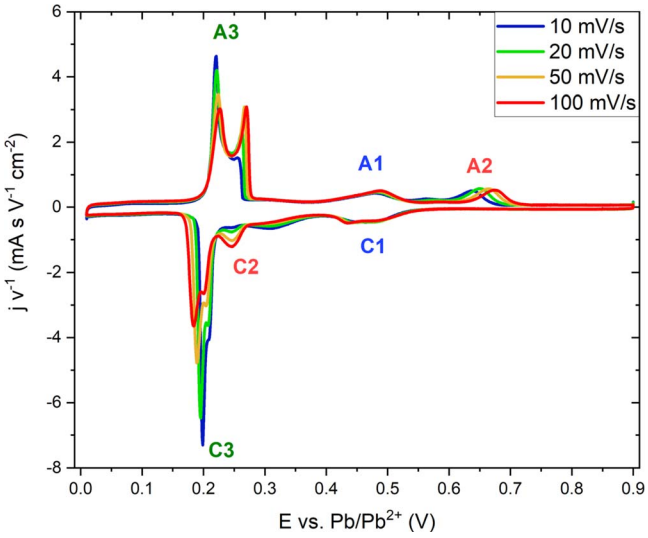


**Figure 3.** Pb UPD CVs on Au (111) in 1 mM $Pb(ClO_4)_2$ and 0.1 M $HClO_4$ solution at different scan rates. The current has been normalized to the surface area and the scan rate.

Figure 2b shows CVs starting from a potential of 0.01 V, at which a complete monolayer of Pb on the surface is formed. Pb is removed from the surface as the potential limit is increased to more positive values. The C3 peak and a hump beyond (in the range of 0.15 V–0.22 V) correspond to the fully formed peaks A3 (yellow line in Fig. 2b). Further scans into the C2 region show no apparent peaks in the anodic direction. As previously observed, the A1 and C1 peaks appear at the same potential of 0.45 V (blue line in Fig. 2b). With the further positive potential limit increase, we can observe the A2 peak formed in the region 0.65 V–0.7 V (purple line in Fig. 2b) and its cathodic C2 counterpart at a more negative potential of 0.25 V, similar to the CV shown in Fig. 2a.

From the results shown in Fig. 2, we can make two observations: (a) C2-A2 peaks irreversibility can be associated with the surface alloying-dealloying at low Pb coverage, and (b) the asymmetry and differences of peaks C3 and A3 can be associated with the dealloying–alloying processes at higher Pb coverage. The CVs

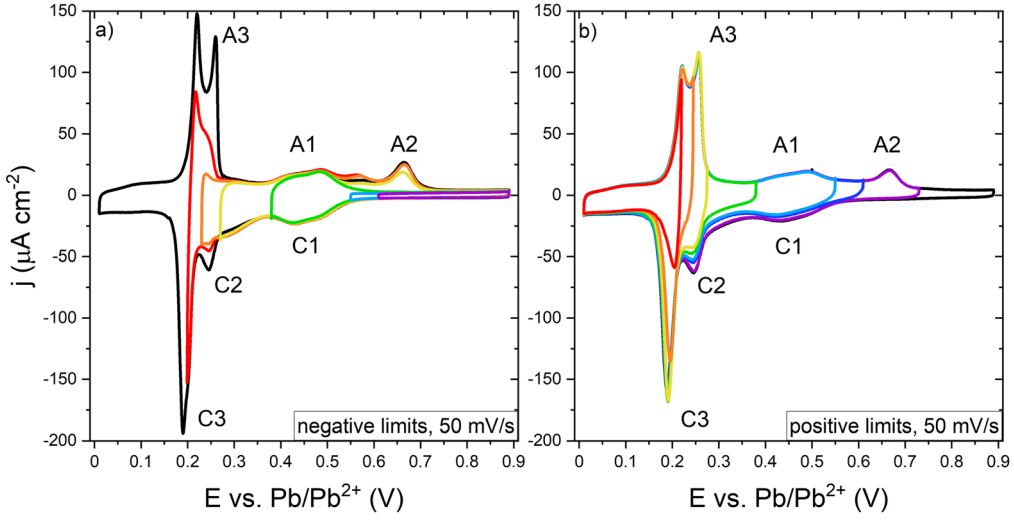


**Figure 2.** CVs of Pb UPD on Au(111) in 1 mM $Pb(ClO_4)_2$ and 0.1 M $HClO_4$ solution with (a) constant positive and varying negative potential limits and (b) constant negative and varying positive potential limits. Scan rate 50 mV $s^{-1}$.

with different scan rates shown in Fig. 3 further support these hypotheses.

In Fig. 3, the potential was cycled with different scan rates ($\Delta E/\Delta t$) from 10 mV $s^{-1}$ to 100 mV $s^{-1}$ between potentials 0.90 V and 0.0 V. For easier comparison, current density was normalized to the scan rate. If the processes are reversible, the positions of peaks do not change with the scan rate. The peak positions change with the scan rate for the irreversible processes (often due to the kinetics effects).

In this system, the positions, and shapes of several peaks, such as C3/A3 and C2/A2, change with scan rates. This suggests a kinetically controlled formation and stripping of Pb on the (111)-oriented features. A more detailed analysis of the main features of the CVs changing with the scan rates includes:

(1) The peak A2 position changes to more positive potentials with the increase of the scan rate. The corresponding cathodic peak C2, at around 0.30 V–0.25 V, changes from a wave (no peak) at low scan rates to a well-defined peak at higher scan rates.
(2) The double (split) peaks of A3 have the same potential separation for all scan rates. However, the splitting of the counterpart peak C3 is observed only at slower scan rates.
(3) The ratio of the two A3 peaks changes and the peak at the more positive potential becomes higher at higher scan rates. Similar peak separations during UPD processes are usually interpreted as the processes on energetically different surface sites, such as steps (at the more positive potentials) and terraces (at the more negative potentials). The changes observed in this system could be understood similarly but cannot be explained entirely by this interpretation. The comparison with A2 and C2 peak behavior suggests that the significant irreversibility could be attributed to the processes with different energetics, such as surface alloying, which could be a pathway dependent.

We analyzed the charge (coverage in percentages) corresponding to the characteristic Pb UPD peaks obtained by integrating CVs with different scan rates shown in Fig. 3. The results are presented in Table I. The total charge density of the cathodic part is consistently higher than the anodic by 2%–15%, as reported before.[14] The charge difference between cathodic and anodic scans is also scan rate sensitive with the largest difference observed at the slowest scan rate. The reason for this is the electrocatalytic effect of Pb UPD on the oxygen reduction reaction (background reaction) in this system previously shown by K. Juttner[74] and Chen et al.[26] The theoretical charge corresponding to the flat Pb monolayer deposited on Au(111) single crystal is 302 $\mu$C $cm^{-2}$. Higher values measured than the theoretical one are due to the surface structure (roughness factor <1.1)[11,15] as well as the mentioned background reaction contribution.

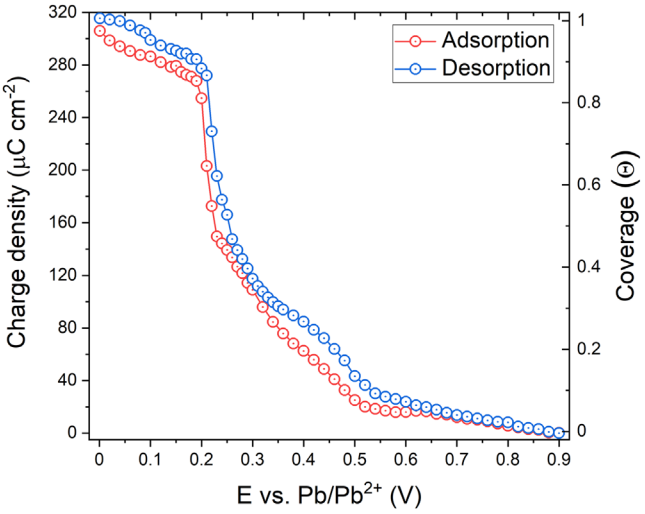


**Figure 4.** Adsorption and desorption isotherms of Pb UPD on Au (111) in 1 mM $Pb(ClO_4)_2$ and 0.1 M $HClO_4$ solution.

Charges under cathodic peaks C1 and their anodic counterparts A1 indicate similar coverage (13%–15%) for all scan rates, as shown in Table I. However, the coverages of peaks C2 and A2 are higher for the low scan rate which is consistent with the assumption that these peaks are associated with the removal of the "trapped" Pb in the top surface (surface alloy). Slower scans allow more time for the slower processes to take place and be better observed. On the contrary, the total coverages of C3 and A3 peaks decrease with the decreasing scan rate.

The potential-dependent charge and coverage (in fractions of ML) of the Pb UPD have been measured by chronoamperometry (CA). The integration of the current-time transients obtained by potential steps from 0.90 V (bare Au, 0 ML) to selected potentials in steps of 0.02 V up to 0.0 V (full Pb coverage, 1 ML) and back from 0.0 V to 0.90 V, are presented in Fig. 4 as the adsorption and desorption isotherms respectively.

The shape of the isotherms agrees with those previously reported in the literature.[11,15] The isotherms show a linear coverage increase in the range 0.90 V (0 ML)–0.50 V (0.1 ML), followed by a steeper nonlinear deposition from 0.50 V to 0.25 V, followed by an almost vertical increase to 1 ML deposition. The distinct, almost step-wise, increase (resembling a first-order phase transition) was modelled by K. Engelsmann et al.[15] with Frumkin isotherm, suggesting a strong lateral attraction between Pb atoms. The maximum deposition charge was measured as 315 ± 20 $\mu$C $cm^{-2}$, which agrees with the results obtained by CV integration shown in Table I.

**Table I. The charge density and the fraction of 1 ML coverage (in %) of Pb for each characteristic UPD peak. The data are compared for 10, 20, 50 and 100 mV $s^{-1}$ for CVs shown in Fig. 3. Total cathodic charge (labelled C) and anodic charge (labelled A) are also included for comparison.**

| | Deposition Peaks | | | | Stripping Peaks | | | |
|---|---|---|---|---|---|---|---|---|
| | $q(\pm5)\mu$C $cm^{-2}$ | | | | $q(\pm5)\mu$C $cm^{-2}$ | | | |
| | $\theta(\pm2)$% | | | | $\theta(\pm2)$% | | | |
| Scan rate (mV $s^{-1}$) | C | C1 | C2 | C3 | A | A1 | A2 | A3 |
| 10 | 336 | 48 | 67 | 161 | 282 | 37 | 52 | 145 |
| | | 14% | 20% | 48% | | 13% | 19% | 51% |
| 20 | 326 | 47 | 58 | 170 | 301 | 40 | 52 | 157 |
| | | 15% | 18% | 52% | | 13% | 17% | 52% |
| 50 | 318 | 45 | 49 | 177 | 305 | 39 | 50 | 164 |
| | | 14% | 15% | 56% | | 13% | 16% | 54% |
| 100 | 315 | 46 | 45 | 182 | 309 | 42 | 47 | 171 |
| | | 15% | 14% | 58% | | 14% | 15% | 56% |

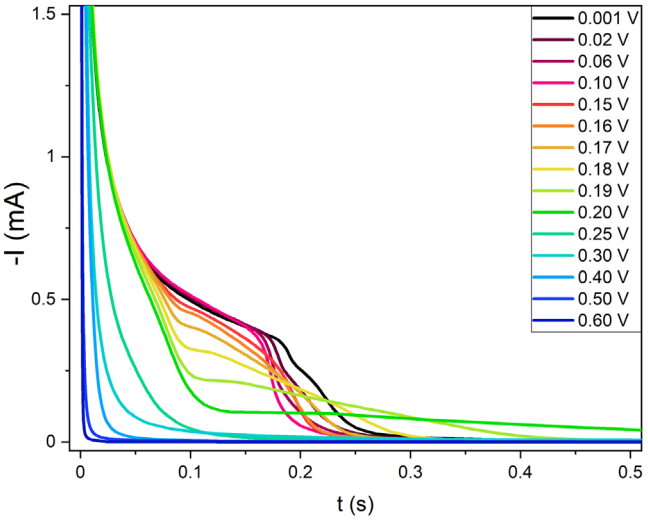


**Figure 5.** Selected cathodic current-time transients after stepping from 0.9 V to different potentials in the Pb UPD on Au(111) region marked in the legend.

Selected current-time transients of Pb deposition during potential steps from 0.9 V (0 ML) up to 0.001 V (1 ML) are shown in Fig. 5. A clear difference between the transients indicates the potential dependence on various competing processes, such as homogenous nucleation and growth or surface alloying. Another interesting observation is that the nucleation time is not proportional to the polarization potential.

The analysis of the cathodic current-time transients shown in Fig. 5 (and those in Fig. S4) can be summarized as follows:

i) the fastest deposition occurs at low coverages, stepping to potentials from 0.6 V up to 0.25 V (from 0 to 0.5 ML). The current reaches zero in less than 0.1 s, and the deposition time increases with the increase of the deposited charge.
ii) at the potential of 0.2 V corresponding to ∼0.85 ML (i.e. in the range of 0.2 V < E < 0.25 V), the deposition transient flattens up, and the current level decays almost ten times slower and reaches zero current after ∼1 s (details shown in Fig. S4b).
iii) between 0.19 V and 0.15 V (0.9 ML –0.94 ML, light green and red curves in Fig. 5), the current transients reach zero after 0.4 s and 0.2 s, respectively. The deposition time decreases with increasing deposited charge.
iv) for the potentials from 0.10 V to 0.001 V (0.96ML –1ML, pink and black curves in Fig. 5), the current reaches zero after 0.2 s, and the deposition time increases with increasing deposited charge.

To better understand the occurring phenomena at different potentials, we have studied the changes after extended polarization at 0.2 V (0.85 ML, green curve in Fig. 5).

***Extended polarization.***—Extended polarization has been commonly used to demonstrate and study surface alloying between the substrate and the adsorbate. One of the most thoroughly studied systems was Pb/Ag(111),[50–52,54–57] for which extensive polarizations were performed at both low and high coverages of Pb. In contrast to that, there is only one previous study reporting polarization at low and high coverages during Pb UPD on Au(111),[15] where the potential was held at 0.1 V (0.95 ML) and 0.47 V (0.28 ML) for 600 s and 300 s respectively.

Our polarization experiments were conducted at high coverage of Pb (0.85 ML), and the changes are shown in Fig. 6. The potential was held at 0.2 V for 15 min and 60 min, after which the potential was swept to 0.9 V (0 ML) with a scan rate of 10 mV $s^{-1}$. Figure 6a shows CVs over the Pb UPD range before and after extended polarization. The A3 double-peak changes are shown in more detail in Fig. 6b. The peaks changed their shape. The more negative peak decreased in height while the positive one increased with the time of polarization. The overall charge measured under the peaks decreased with polarization time by about 20 $\mu$C $cm^{-2}$, as shown in Table II.

Before polarization, the peak A2 shown in Fig. 6c was a single peak at around 0.6 V. Following the polarization, this peak decreased in height, and a new peak at more positive potentials (of ∼0.1 V) appeared of increasing height with the polarization time. Overall charge under the peak A2 after 60 min increased by almost 30 $\mu$C $cm^{-2}$, as shown in Table II. This result agrees with the charge

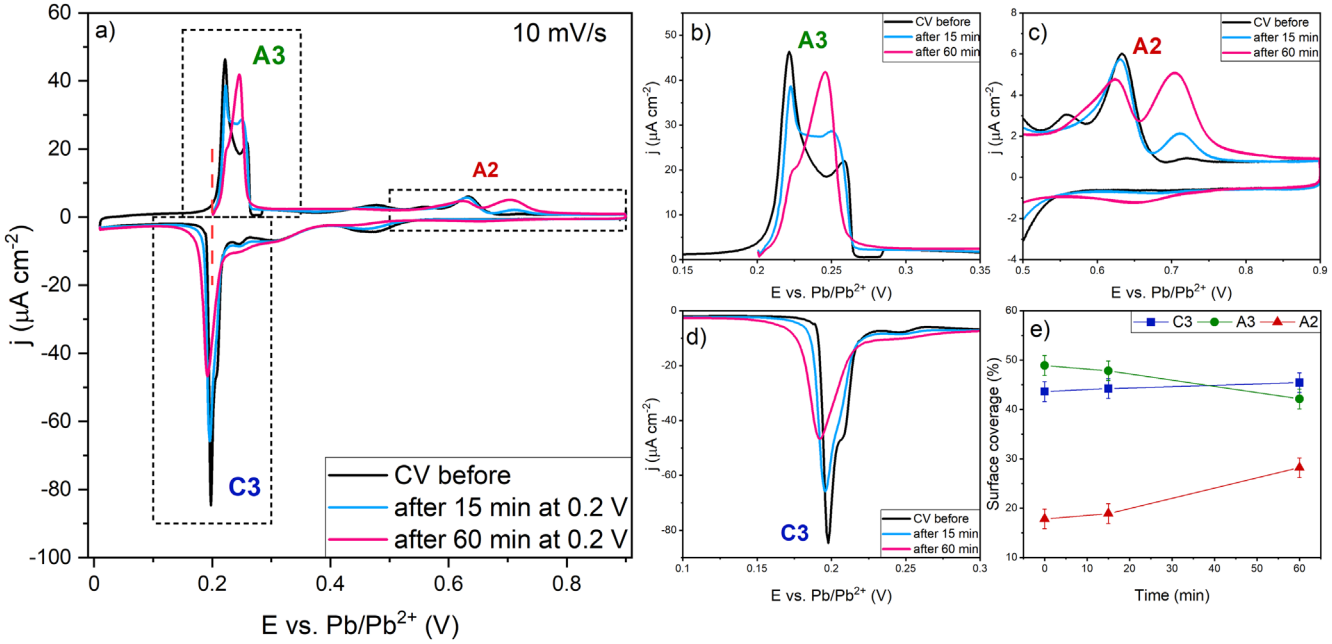


**Figure 6.** CVs of Pb UPD on Au(111) film before and after different times of polarization at 0.2 V (marked by a dashed red line). (a) The view of the whole CV scans. (b), (c), (d) enlarged regions of A3, A2, and C3 peaks, respectively; (e) changes of the Pb ML coverage under the UPD peaks with the time of polarization. Scan rate 10 mV $s^{-1}$.

**Table II. The changes in the charge density of the main UPD peaks with the polarization time at 0.2 V.**

| | q (±5) $\mu$C cm$^{-2}$ | | |
|---|---|---|---|
| Polarization time (min) | A3 | A2 | C3 |
| 0 | 137 | 50 | 144 |
| 15 | 134 | 53 | 146 |
| 60 | 118 | 79 | 150 |

increase and peak splitting reported in the earlier study by K. Engelsmann et al., where the system was polarised at 0.1 V for 600 s.[15] The charge density of A2 reaches a value of 79 $\mu$C cm$^{-2}$ after 60 min of polarization, which is equivalent to the coverage of about 0.28 ML, suggesting 28% of an ML alloyed with the top Au surface. Figure 6d shows the change in the C3 peak following the polarization and anodic scan. The peak decreases significantly in height due to significant broadening, but the overall charge is only slightly increased. The overall changes in the charge density (fraction of 1 ML of Pb) for all main UPD peaks are given in Table II and graphically presented in Fig. 6e.

Similarly to what was shown for the Pb/Ag system, the charges under peak A3 decreased with the polarization time.[50–52,54–57] While this observation indicates surface alloying, there is also an unusual behavior of peak A2. The charge not only increased, but the peak shifted and split. The initially present peak reduced in height, and a new peak formed ∼0.1 V at more positive potentials. The same A2 peak splitting and the charge increase after extended polarization was observed in the early study by K. Engelsmann et al.,[15] which was interpreted as a result of a very stable "surface reconstruction".[15] However, the observed potential shift was not as significant as in our case, possibly due to shorter polarization time and the polarization potential that was 0.1 V more negative than ours.

Following the extended polarization, the surface of the substrate was studied by CVs in the whole range of the Pb UPD, as shown in Fig. S5. It can be observed that the peaks characteristic for Pb UPD on Au(111) were less pronounced and some were even absent. The lack of recovery of the Au substrate indicates that the introduced changes due to polarization were significant (permanent). This result confirms extensive surface alloying between Pb and Au due to polarization at 0.2 V.

***Dynamic alloying.***—We used another technique called "dynamic alloying," which presents successive potential cycling to explore surface alloying further. A similar type of dynamic alloying was used to show alloying in the Ag/Au(111) system,[59,60] where the potential cycling was done either between potentials corresponding to 0 ML and 1 ML coverages[59] or between partial and complete ML coverages.[60] During the dynamic alloying, the changes of UPD peaks shape and magnitude indicated site blocking due to surface alloying.[59,60]

Our approach was similar to the one used by Snyder et al.[60] The potential was cycled between 0.5 V and 0.0 V, corresponding to 0.25 ML and 1 ML Pb coverage, respectively. The potential range was chosen to be below A2, the "dealloying" peak. Our interest was in observing the changes in the magnitude and position of specific UPD peaks resulting from successive deposition and dissolution cycles of Pb within the potential region where the alloying and the dealloying occur.

The results of repeated cycling in the Pb UPD potential region are shown in Fig. 7. The potential was cycled up to 1150 times with a rate of 10 mV s$^{-1}$. Figure 7a shows the changes in peak shapes after numerous cycles in the whole range of Pb UPD. The peaks C1/A1, corresponding to deposition/dissolution at the step edges, were gradually diminishing with the number of cycles, possibly due to the loss or damage of well-defined edges and terraces of Au(111). The A3 peak shown in Fig. 7b decreased in height, changed shape (double-peak structure transformed to one broad peak) and shifted ∼0.01 V to more positive potentials. Figure 7c shows the changes in the A2 peak after the multiple scans. The A2 peak decreased in height, and a new peak formed ∼0.1 V at a more positive potential, similar to what was observed after extended polarization shown in Fig. 6c. The peak C3 changes shown in Fig. 7d were similar to the changes of peak A3. It decreased in magnitude and transformed into one broad peak that shifted negative by ∼0.005 V. The overall changes in the coverage of the main UPD peaks are shown in Fig. 7e. The integrated charge densities (normalized to ECASA of

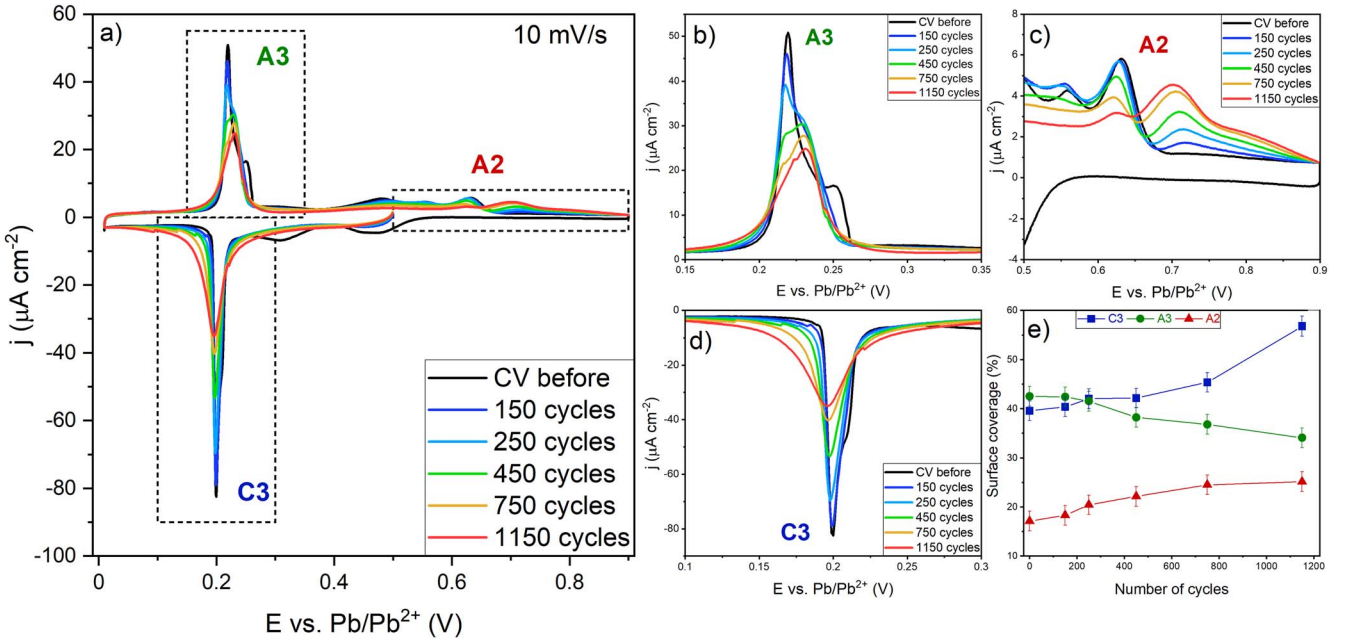


**Figure 7.** CVs of Pb UPD on Au(111) before and after repeated potential cycles between 0.0 V and 0.5 V. (a) The view of the whole CV scan. (b), (c), (d) enlarged regions of A3, A2, and C3 peaks, respectively; (e) changes of the Pb ML coverage under the UPD peaks with the number of cycles. Scan rate 10 mV s$^{-1}$.

**Table III. The changes in the charge density of the main UPD peaks during dynamic alloying (repeated potential cycling) with the number of potential cycles between 0.5 V and 0.0 V.**

| Number of cycles | q (±5) $\mu$C cm$^{-2}$ | | |
|---|---|---|---|
| | C3 | A3 | A2 |
| 0 | 123 | 141 | 57 |
| 150 | 125 | 140 | 61 |
| 250 | 130 | 137 | 68 |
| 450 | 131 | 127 | 73 |
| 750 | 141 | 122 | 81 |
| 1150 | 176 | 113 | 83 |

the initial surface) of the characteristic peaks after the different number of potential cycles are shown in Table III.

The charge density of C3 increased by about 53 $\mu$C cm$^{-2}$ after 1150 cycles. One possible explanation is the surface roughening due to alloying, which increased the surface area. On the other hand, the charge density of A3 decreased by about 28 $\mu$C cm$^{-2}$ after 1150 cycles. However, an interesting observation is that the total charge density of two anodic peaks (A3 + A2) generally was constant ($\sim$200 $\mu$C cm$^{-2}$).

The charge density of A2 increased with the number of cycles. It reached a value of 83 $\mu$C cm$^{-2}$ after 1150 cycles, equivalent to $\sim$0.3 ML coverage (30%) of Pb alloyed with the Au top surface. The alloying studies on a similar system Pb/Ag(111) showed that $\sim$10% of the alloyed Pb ML can block the Ag surface altogether.[52]

After "dynamic alloying," the surface of the Au substrate was studied by CVs in the whole range of the Pb UPD, as shown in Fig. S6. It was observed that the peaks characteristic for Pb UPD on Au (111) were changed (such as C3/A3) or even absent (such as peaks C1/A1 and A2). The lack of recovery of the Au substrate indicated that the surface changes created by repeated potential cycling are permanent, which agrees with the surface alloying of Pb and Au.

## Conclusions

In this work, we revisited the well-known system of Pb UPD on Au(111), focusing on the processes of surface alloying, demonstrated by the irreversibility of the deposition and dissolution peaks, which have been a subject of various interpretations in the past. We presented the electrochemical investigations during constant potential polarization and numerous potential cycles in the region of high Pb coverage. The following conclusions are drawn from the study:

(1) Surface alloying in this system is manifested by "dealloying peak" A2. On the freshly prepared Au surface, A2 is a single peak whose position and charge depend on the scan rate. The corresponding charge/coverage is equivalent to $\sim$0.15–0.2 ML (measured for scan rates 10 mV s$^{-1}$ – 100 mV s$^{-1}$).

(2) After the potential polarization at 0.85 ML of Pb (at 0.2 V) for 15 min, changes in A2 peak shape were observed, with only a slight change of the charge under the peak (change from 50 $\mu$C cm$^{-2}$ – 58 $\mu$C cm$^{-2}$). However, after 60 min of polarization, the charge under the A2 peak increased to 79 $\mu$C cm$^{-2}$, equivalent to the coverage of $\sim$0.28ML of Pb alloyed with the Au surface. Prolonged polarization also resulted in a more negative peak potential shift of $\sim$0.1 V.

(3) After 1150 potential cycles between 0.5 V and 0.0 V (between 0.25 ML and 1 ML Pb), the charge under the A2 peak increased from 57 $\mu$C cm$^{-2}$ to 83 $\mu$C cm$^{-2}$, equivalent to the coverage of about 0.30 ML Pb coverage.

The results showed similar voltammetric changes and magnitude of surface alloying following numerous potential cycles and constant potential polarization. The two experimental approaches resulted in unrecoverable, i.e. irreversible, changes on the Au(111) surface. Further work using the in situ STM will determine the surface structure evolution and understanding of the mechanism of the Pb/Au surface alloying during potentiostatic and potentiodynamic alloying.

## Acknowledgments

A.S and N.V. acknowledge the support of the Bristol Centre for Functional Nanomaterials and the financial support of the U.K. Engineering and Physical Sciences Research Council (EPSRC) as part of grant code EP/L016648/1. We thank Prof. Neil A. Fox for UHV deposition of Au-films on glass, and Dr Ross S. Springell and Dr Jacek M. Wasik for XRD characterisation.

## Data Availability Statement

All underlying data to support the conclusions are provided within this paper and the Supplementary Data file.

## ORCID

Alicja Szczepanska https://orcid.org/0000-0002-7829-6978
Natasa Vasiljevic https://orcid.org/0000-0002-7515-9708

## References

1. A. V. Ruban, H. L. Skriver, and J. K. Norskov, *The Chemical Physics of Solid Surfaces*, ed. D. P. Woodruff (Elsevier, New York, NY) 10, p. 1 (2002).
2. J. Tersoff, *Phys. Rev. Lett.*, **74**, 434 (1995).
3. J. P. Biberian and G. E. Rhead, *J. Phys. F: Met. Phys.*, **3**, 675 (1973).
4. H. C. Snyman and F. W. Boswell, *Surf. Sci.*, **41**, 21 (1974).
5. J. Perdereau, J. P. Biberian, and G. E. Rhead, *J. Phys. F: Met. Phys.*, **4**, 798 (1974).
6. J. Biberian, *Surf. Sci.*, **74**, 437 (1978).
7. A. Crepaldi, S. Pons, E. Frantzeskakis, F. Calleja, M. Etzkorn, A. P. Seitsonen, K. Kern, H. Brune, and M. Grioni, *Phys. Rev. B*, **87**, 115138 (2013).
8. C. Pariset, M. Galtier, and M. Gasgnier, *Thin Solid Films*, **29**, 325 (1975).
9. E. Bauer, *Appl. Surf. Sci.*, **11–12**, 479 (1982).
10. J. W. Shin, U. Bertocci, and G. R. Stafford, *The Journal of Physical Chemistry C*, **114**, 7926 (2010).
11. J. Nutariya, J. Velleuer, W. Schwarzacher, and N. Vasiljevic, *ECS Trans.*, **28**, 15 (2010).
12. R. Adzic, E. Yeager, and B. Cahan, *J. Electrochem. Soc.*, **121**, 474 (1974).
13. J. W. Schultze and D. Dickertmann, *Surf. Sci.*, **54**, 489 (1976).
14. A. Hamelin, *J. Electroanal. Chem. Interfacial Electrochem.*, **101**, 285 (1979).
15. K. Engelsmann, W. J. Lorenz, and E. Schmidt, *J. Electroanal. Chem. Interfacial Electrochem.*, **114**, 1 (1980).
16. A. Hamelin and A. Katayama, *J. Electroanal. Chem. Interfacial Electrochem.*, **117**, 221 (1981).
17. D. Rath, *J. Electroanal. Chem.*, **150**, 521 (1983).
18. M. Alvarez-Rizatti and K. Jüttner, *J. Electroanal. Chem. Interfacial Electrochem.*, **144**, 351 (1983).
19. A. Hamelin, *J. Electroanal. Chem. Interfacial Electrochem.*, **165**, 167 (1984).
20. A. Hamelin and J. Lipkowski, *J. Electroanal. Chem. Interfacial Electrochem.*, **171**, 317 (1984).
21. J. P. Ganon and J. Clavilier, *Surf. Sci.*, **145**, 487 (1984).
22. M. P. Green, M. Richter, X. Xing, D. Scherson, K. J. Hanson, P. N. Ross, R. Carr, and I. Lindau, *J. Microsc.*, **152**, 823 (1988).
23. M. Green, K. Hanson, D. Scherson, X. Xing, M. Richter, P. Ross, R. Carr, and I. Lindau, *J. Phys. Chem.*, **93**, 2181 (1989).
24. M. P. Green, K. J. Hanson, R. Carr, and I. Lindau, *J. Electrochem. Soc.*, **137**, 3493 (1990).
25. M. P. Green and K. J. Hanson, *Surf. Sci.*, **259**, L743 (1991).
26. C. H. Chen, N. Washburn, and A. A. Gewirth, *J. Phys. Chem.*, **97**, 9754 (1993).
27. M. F. Toney, J. G. Gordon, M. G. Samant, G. L. Borges, and O. R. Melroy, *J. Phys. Chem.*, **99**, 4733 (1995).
28. M. Seo and M. Yamazaki, *J. Electrochem. Soc.*, **151**, E276 (2004).
29. G. R. Stafford and U. Bertocci, *The Journal of Physical Chemistry C*, **111**, 17580 (2007).
30. Q. Yuan, A. Tripathi, M. Slavkovic, and S. R. Brankovic, *Z. Phys. Chem.*, **226**, 965 (2012).
31. M. Seo, *Electro-Chemo-Mechanical Properties of Solid Electrode Surfaces*, ed. M. Seo (Springer, Singapore) p. 103 (2020).
32. E. Herrero, L. J. Buller, and H. D. Abruña, *Chem. Rev.*, **101**, 1897 (2001).
33. Y. Liu, S. Bliznakov, and N. Dimitrov, *J. Phys. Chem. C*, **113**, 12362 (2009).
34. T. Takamura and K. Takamura, *Surface Electrochemistry: Advanced Methods and Concepts*, ed. T. Takamura and A. Kozawa (Japan Scientific Societies Press, Tokyo) p. 229 (1978).
35. M. G. Samant, M. F. Toney, G. L. Borges, L. Blum, and O. R. Melroy, *J. Phys. Chem.*, **92**, 220 (1988).
36. E. D. Chabala, B. H. Harji, T. Rayment, and M. D. Archer, *Langmuir*, **8**, 2028 (1992).
37. N. J. Tao, J. Pan, Y. Li, P. I. Oden, J. A. DeRose, and S. M. Lindsay, *Surf. Sci.*, **271**, L338 (1992).

38. D. Carnal, P. Oden, U. Muller, E. Schmidt, and H. Siegenthaler, *Electrochim. Acta*, **40**, 1223 (1995).
39. I. Oh, A. Gewirth, and J. Kwak, *Langmuir*, **17**, 3704 (2001).
40. J. W. Yan, J. Tang, Y. Y. Yang, J. M. Wu, Z. X. Xie, S. G. Sun, and B. W. Mao, *Surf. Interface Anal.*, **32**, 49 (2001).
41. J.-W. Yan, J.-M. Wu, Q. Wu, Z.-X. Xie, and B.-W. Mao, *Langmuir*, **19**, 7948 (2003).
42. T. P. Moffat, *J. Phys. Chem. B*, **102**, 10020 (1998).
43. R. V. Kukta, N. Vasiljevic, N. Dimitrov, and K. Sieradzki, *Phys. Rev. Lett.*, **95**, 186103 (2005).
44. M. D. Lay and J. L. Stickney, *J. Am. Chem. Soc.*, **125**, 1352 (2003).
45. C. Schlaup and S. Horch, *Surf. Sci.*, **632**, 126 (2015).
46. S. G. García, D. R. Salinas, and G. Staikov, *Surf. Sci.*, **576**, 9 (2005).
47. G. Staikov, S. García, and D. Salinas, *ECS Trans.*, **25**, 3 (2010).
48. T. Brunt, T. Rayment, S. OShea, and M. Welland, *Langmuir*, **12**, 5942 (1996).
49. C. Friesen, N. Dimitrov, R. C. Cammarata, and K. Sieradzki, *Langmuir*, **17**, 807 (2001).
50. H. Siegenthaler and K. Jüttner, *Electrochim. Acta*, **24**, 109 (1979).
51. T. Vitanov, A. Popov, G. Staikov, E. Budevski, W. J. Lorenz, and E. Schmidt, *Electrochim. Acta*, **31**, 981 (1986).
52. A. Popov, N. Dimitrov, O. Velev, T. Vitanov, E. Budevski, E. Schmidt, and H. Siegenthaler, *Electrochim. Acta*, **34**, 265 (1989).
53. A. Popov, N. Dimitrov, D. Kashchiev, T. Vitanov, and E. Budevski, *Electrochim. Acta*, **34**, 269 (1989).
54. N. Dimitrov, A. Popov, D. Kashchiev, T. Vitanov, and E. Budevski, *Electrochim. Acta*, **36**, 1259 (1991).
55. N. Dimitrov, A. Popov, T. Vitanov, and E. Budevski, *Electrochim. Acta*, **36**, 2077 (1991).
56. N. Dimitrov, A. Popov, D. Kashchiev, and T. Vitanov, *Electrochim. Acta*, **39**, 957 (1994).
57. A. Popov, N. Dimitrov, T. Vitanov, D. Kashchiev, and E. Budevski, *Electrochim. Acta*, **40**, 1495 (1995).
58. H.-C. Wu and S.-L. Yau, *J. Phys. Chem. B*, **105**, 6965 (2001).
59. V. Rooryck, F. Reniers, C. Buess-Herman, G. A. Attard, and X. Yang, *J. Electroanal. Chem.*, **482**, 93 (2000).
60. J. D. Snyder and J. D. Erlebacher, *Langmuir*, **25**, 9596 (2009).
61. R. Vidu and S. Hara, *Scr. Mater.*, **41**, 617 (1999).
62. R. Vidu and S. Hara, *J. Electroanal. Chem.*, **475**, 171 (1999).
63. R. Vidu and S. Hara, *Surf. Sci.*, **452**, 229 (2000).
64. R. Vidu, N. Hirai, and S. Hara, *Phys. Chem. Chem. Phys.*, **3**, 3320 (2001).
65. H. Bort, K. Jüttner, W. J. Lorenz, and G. Staikov, *Electrochim. Acta*, **28**, 993 (1983).
66. V. Vicente and S. Bruckenstein, *J. Electroanal. Chem.*, **82**, 187 (1977).
67. K. Gossner and E. Mizera, *J. Electroanal. Chem. Interfacial Electrochem.*, **125**, 359 (1981).
68. L. A. Kibler, M. Kleinert, V. Lazarescu, and D. M. Kolb, *Surf. Sci.*, **498**, 175 (2002).
69. G. Wu, S. Bae, A. Gewirth, J. Gray, X. Zhu, T. Moffat, and W. Schwarzacher, *Surf. Sci.*, **601**, 1886 (2007).
70. H. Siegenthaler and K. Jüttner, *J. Electroanal. Chem. Interfacial Electrochem.*, **163**, 327 (1984).
71. S. Trasatti and O. A. Petrii, *J. Electroanal. Chem.*, **327**, 353 (1992).
72. H. Angerstein-Kozlowska, B. E. Conway, A. Hamelin, and L. Stoicoviciu, *Electrochim. Acta*, **31**, 1051 (1986).
73. H. Angerstein-Kozlowska, B. E. Conway, A. Hamelin, and L. Stoicoviciu, *J. Electroanal. Chem. Interfacial Electrochem.*, **228**, 429 (1987).
74. K. Juttner, *Electrochim. Acta*, **29**, 1597 (1984).